Ionic charge dependence of the internal conversion coefficient and nuclear lifetime of the first excited state in ^{125}Te

F. Attallah,[1,*] M. Aiche,[1] J. F. Chemin,[1] J. N. Scheurer,[1] W. E. Meyerhof,[2] J. R. Grandin,[3] P. Aguer,[4] G. Bogaert,[4] C. Grunberg,[5] J. Kiener,[4] A. Lefebvre,[4] and J. P. Thibaud[4]

[1]*Centre d'Etudes Nucléaires de Bordeaux-Gradignan, IN2P3-CNRS, Université de Bordeaux, Boîte Postale 117, F-33175 Gradignan, France*

[2]*Department of Physics, Stanford University, Stanford, California 94305*

[3]*Centre Interdisciplinaire de Recherche avec les Ions Lourds, CEA-CNRS, Boîte Postale 5133, F-14040 Caen, France*

[4]*Centre de Spectrométrie Nucléaire et de Spectrométrie de Masse, IN2P3-CNRS, Université d'Orsay, F-91405 Orsay, France*

[5]*Grand Accélérateur National d'Iond Lourds, Boîte Postale 5027, F-14021 Caen, France*

(Received 21 October 1996)

We have studied the ionic charge state dependence of the nuclear lifetime of the 35.5-keV first excited state of ^{125}Te. We found for the 47^+ and 48^+ ions, 400 and 670 % variations with respect to the neutral-atom half-life (1.49 ns). These unusually large effects are due to the energetic blocking of the *K*-shell internal conversion as the charge state increases past 47^+. For the 46^+, we suggest a new internal conversion mode without any electron emission into the energy continuum. [S0556-2813(97)00104-0]

PACS number(s): 23.20.Nx, 21.10.Tg, 27.60.+j

I. INTRODUCTION

Although the dependence of the nuclear lifetime ($T_{1/2}$) or decay constant (λ) on the extranuclear environment had been investigated for a long time, only very small variations ($\Delta\lambda/\lambda \sim 10^{-3}$) were found [1]. The revival of interest in this field in recent years is due to accelerator developments which make it possible to induce drastic changes in the extranuclear environment by ionizing the *inner*atomic shells. Such processes, as β decay, electron capture, and internal conversion (IC), all of great interest for astrophysics [2], are very sensitive to the electronic density in the vicinity of the nucleus. However, Ulrickson *et al.* [3] found that the removal of up to ten electrons did not affect significantly the lifetime of the 77-keV level in ^{197}Au. Recently, two experiments have demonstrated that in highly ionized atoms the electronic configurations can have a drastic effect on the nuclear decay. In the first experiment, Jung *et al.* [4] found a spectacular decrease of the ^{163}Dy half-life from $T_{1/2}=\infty$ (stable) in a neutral atom to $T_{1/2}=50d$ in the bare nucleus, which is the experimental proof of *bound β decay*, a process previously suggested by Daudel *et al.* [5]. The second experiment, by Phillips *et al.* [6], concerns the measurement of the internal conversion coefficient (ICC) of the 14.4-keV excited state in ^{57}Fe ions with few electrons. A 20% increase was observed in the decay rate of Li-like ions, compared to the decay rate of the neutral atom.

In this paper we report on a several-hundred-percent variation of the internal conversion coefficient and the concomitant lifetime in ^{125}Te with the ionic charge state. A first account of this work has been given in a previous paper [7]. The present paper presents in detail the experimental method and gives a complete account of the data analysis and interpretation.

*Present address: GSI, Postfach 110552, D-64291 Darmstadt, Germany.

II. GENERAL CONSIDERATIONS

In the neutral ^{125}Te atom, the first excited nuclear level (35.492 keV, $3/2^+$) decays by an almost pure $M1$ transition (99.96%) with a half-life of 1.486 ns [8–10]. The main decay mode of this level is by internal conversion (IC) on the K, L, and M shells. The corresponding internal conversion coefficients (ICC) in the neutral atom are respectively equal to [11]: $\alpha_K^0=11.987, \alpha_{L_1}^0=1.461, \alpha_{L_{2,3}}^0=0.145, \alpha_M^0=0.319, \alpha_T^0=13.912$, where α_T^0 is the total ICC and L_1, L_2, and L_3 refer respectively to the subshell $2s$, $2p_{1/2}$, and $2p_{3/2}$. The measured half-life $T_{1/2}^0$ in the neutral atom is related to the partial radiative decay width of this level Γ_γ^0 through the expression

$$T_{1/2}^0=\frac{\hbar \ln 2/\Gamma_\gamma^0}{1+\alpha_K^0+\alpha_L^0+\alpha_M^0}. \tag{2.1}$$

The removal of outer-shell electrons has two different effects on the IC decay process. (i) It modifies the electron number in the different shells; the corresponding ICC diminishes and vanishes at the limit of empty shells [3,6,12]. (ii) It increases the effective Coulomb field seen by the outer electrons and increases the binding energy of the remaining electrons. The binding energy of the K-shell electron has been calculated using relativistic wave functions for Te ions with charge states ranging between 44^+ and 51^+. Some of these values are listed in Table I. Only small deviations in these values are seen when different electronic wave functions are used.

For one particular charge state, called hereafter the *critical charge state* Q_c, the binding energy of the K-shell electron ($E_{B_K}^{Q_c}$) becomes larger than the available nuclear transition energy (ω_γ). In this case, in the usual IC process, with the emission of a bound electron into the energy continuum, the K-shell ionization by IC becomes energetically impossible despite the presence of the two K-shell electrons. Consequently the half-life should increase by a factor corre-

TABLE I. Electronic configurations and K-shell binding energies (E_B^K) of ^{125}Te for various ionic charge states. Boldfaced values of E_B^K exceed 35.492 keV.

Charge state	Config.	E_B^K (keV) Ref. [13]	Ref. [26]	Ref. [27]
0	(neutral)	31.81[a]		
44	$(2s^2 2p^4)$	35.262	35.27	35.263
45	$(2s^2 2p^3)$	35.581	35.58	35.580
46	$(2s^2 2p^2)$	35.909	35.90	35.908
47	$(2s^2 2p)$	36.256	36.23	36.252
48	$(2s^2)$	36.599	36.57	36.602

[a]From Ref. [28].

sponding to the suppression of α_K in Eq. (2.1). Using the K-shell binding energy calculations in Table I, we obtain $Q_c = 45$.

The half-life of the first excited nuclear state of ^{125}Te ($T_{1/2}^Q$) as a function of Q can be related to the neutral-atom half-life $T_{1/2}^0$ by

$$T_{1/2}^Q = T_{1/2}^0 \frac{1+\alpha_T^0}{1+\alpha_T^Q}, \tag{2.2}$$

where

$$\alpha_T^0 = \alpha_K^0 + \alpha_L^0 + \alpha_M^0, \tag{2.3}$$

$$\alpha_T^{Q \geq Q_c} = \alpha_L^{Q \geq Q_c} \tag{2.4}$$

since the M shell is empty for $Q \geq Q_c$. The superscripts above refer to the ionic charge state of Te. One finds for the half-life of He-like ^{125}Te a value $T_{1/2}^{50^+} = 22.17$ ns compared to $T_{1/2}^0 = 1.486$ ns.

III. EXPERIMENT

Our experimental technique follows closely that of Phillips *et al.* [6]. A beam of 27-MeV/u ^{125}Te^{38+} ions (corresponding to a velocity of 7.18 cm/ns), accelerated at GANIL, impinged on a 1-mg/cm^2 target of ^{232}Th in order to strip the ions and to Coulomb excite the nuclei.

Figure 1 shows the experimental setup. It can be separated into three parts. The first part serves to produce the Coulomb interaction of the Te ions with the target and to define the scattering angle. The second part separates of the Te ion trajectories according to their charge states by means of the magnetic field of the dispersive spectrometer SPEG [14]. This spectrometer consists of two magnetic dipoles separated by a drift space. The mean trajectory radius in the dipoles is 2.5 m. A quadrupole lens at the exit of the dipoles is tuned to obtain parallel trajectories before entering the third, detec-

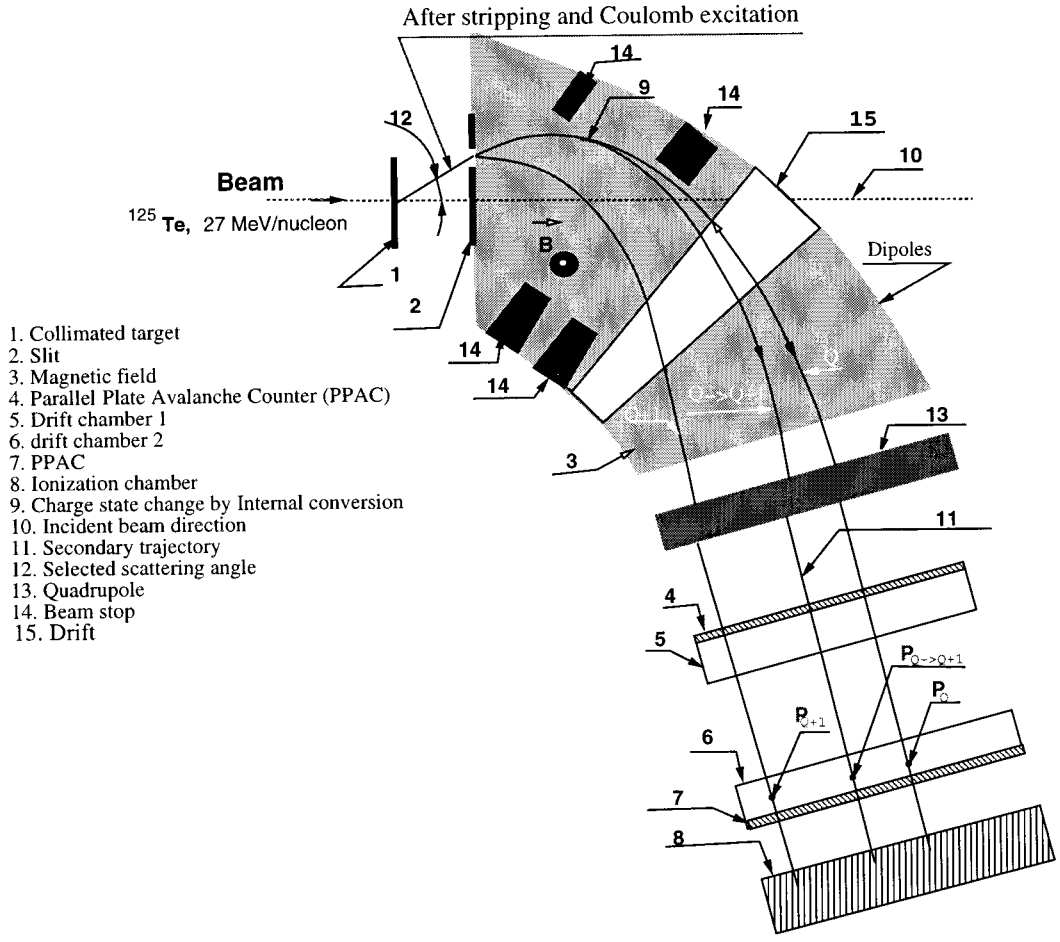

FIG. 1. Experimental setup.

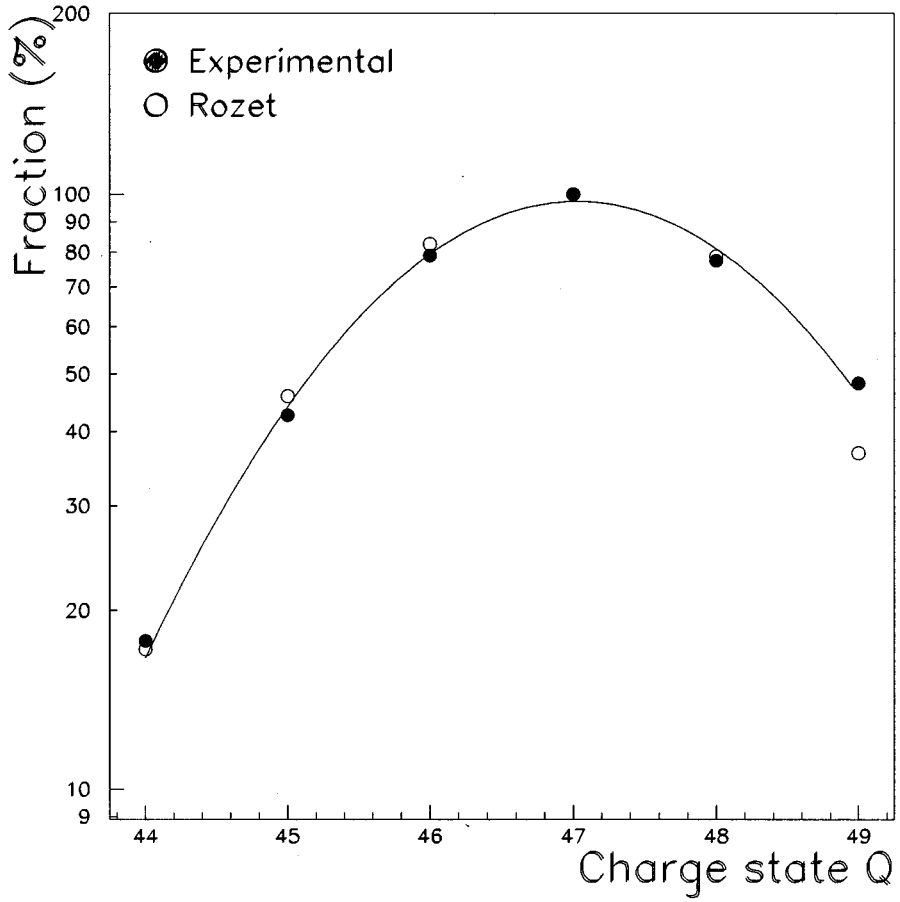

FIG. 2. Charge state distribution of ^{125}Te ions at the exit of the 1-mg/cm^2 Th target. The experimental distribution is superimposed on the theoretical charge state distribution from [15].

tion, and trajectory analysis part at the end of the spectrometer.

The target is mounted as shown in Fig. 1, at a distance $d=11$ cm in front of the first dipole, which corresponds to a time of flight $t_d \simeq T^0_{1/2}$. This time allows for, (i) the feeding of the first nuclear excited state through the deexcitation of Coulomb excited higher levels in ^{125}Te with half-lives $<10^{-9}$ s; (ii) the rearrangement of the atomic electrons to the ground-state configuration, except for a few metastable configurations (see Sec. IV).

The scattering angle ($\theta_{\rm Cex}$) of Te ions is defined by a system consisting of a rectangular aperture 1-mm wide and 25-mm high in front of the target (not shown in Fig. 1) and a movable slit, 0.1-mm wide and 50-mm high, mounted in the entrance plane of the magnetic field. The remaining space of the entrance plane was completely masked. This arrangement defines the scattering angle to $\Delta\theta=\pm 0.2^0$. After the time t_d, the scattered ions with different charge states (43^+-50^+) enter the magnetic field and follow trajectories defined by (i) the magnetic rigidity, (ii) the incident angle θ_0 and position X_0 in the magnetic field relative to the spectrometer optical axis, (iii) the charge state Q and momentum P. These ions reach the ionization chamber after a time of $\sim$150 ns upon leaving the target. The travel time inside the magnetic field is $\sim$70 ns, which indicates the order of magnitude of the lifetime limit in the present method.

The horizontal (X) and vertical (Y) positions of the ^{125}Te ions at the exit of the last quadrupole are detected event by event in two identical drift chambers, separated by a distance of 1.9 m. From these parameters the corresponding horizontal (θ) and vertical (ϕ) angular distributions of ^{125}Te ions are computed. The coincidence signal between two parallel plate avalanche counters (PPAC), joined to each drift chamber, and the cyclotron high frequency provides a fast trigger for the acquisition system. To measure the energy of the scattered beam, the ions are stopped in an ionization chamber which has an energy resolution of 1.7%.

As the normal target position and beam focus of SPEG are located 3 m away from the first dipole [14], the present position of the target requires a special beam focusing. Also, in this situation, the spectrometer is no longer achromatic and the impact position of the ions in each drift chamber becomes very dependent upon the horizontal incident angle θ_0 and position X_0 [12]. For the second drift chamber, one finds $\delta X/\delta\theta_0 \simeq 0.30$ cm/mrad, where X is the horizontal ion position in the chamber. Also, the spectrometer dispersion is affected; one finds $\Delta X/\delta P/P=8.53$, 8.02, and 7.68 cm % for $\theta_0=-1.4$, $+0.6$, $+2.5°$, respectively. These values are in excellent agreement with those obtained by the simulation discussed below. The angle θ_0 is limited to $\sim 3°$ by beam stops mounted inside SPEG (Fig. 1) which decrease drastically the spectrometer transmission beyond this angle. Therefore, the scattering angle in the experiment was fixed to $\theta_{\rm Cex}=2.6°$, as a compromise between an optimum spectrometer transmission and a maximum Coulomb excitation probability. This angle is much smaller than the nuclear grazing angle (6°).

The 1-mg/cm^2 ^{232}Th target produces an ion energy loss

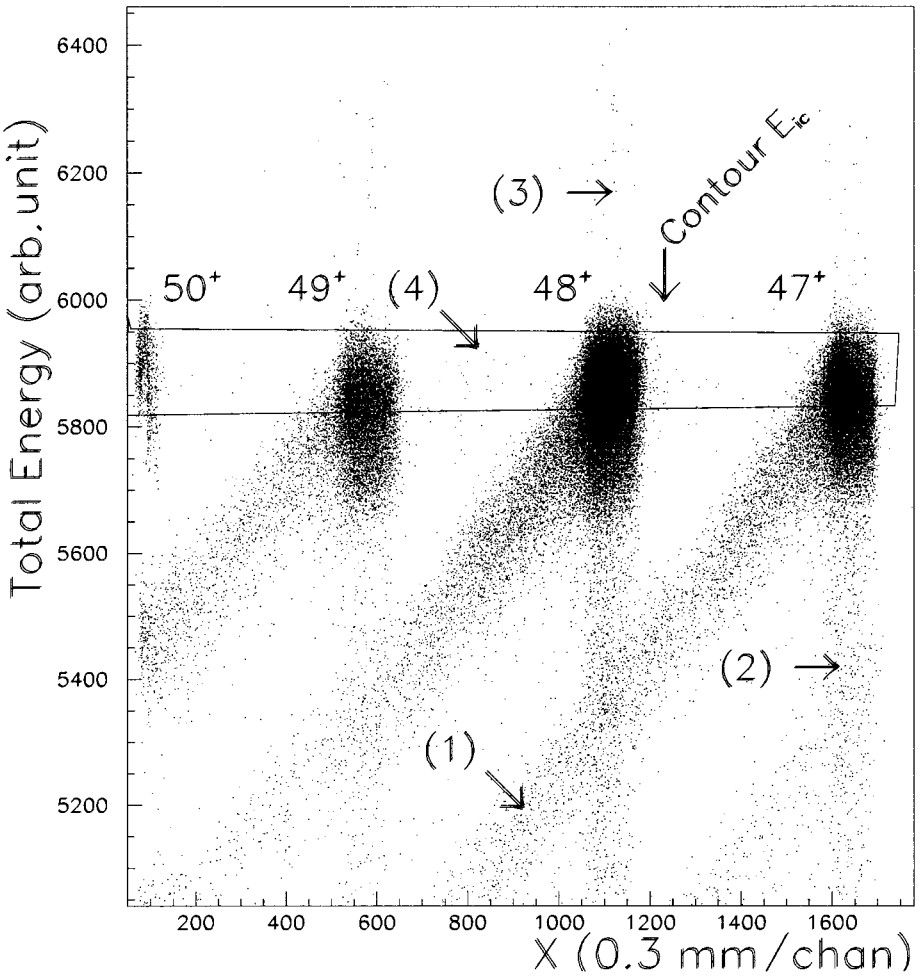

FIG. 3. Total energy versus the horizontal position (X) in the second drift chamber for scattered ions at $\theta_{\mathrm{Cex}}=2.6°$. There are four different kinds of events as labeled, next to the *parent* peaks of the charge states 47, 48, and 49 (see text). The rectangle shows the energy-position contour (E_{ic}) used to gate the elastic events.

of 17.2 MeV, and broadens the relative full width at half maximum of the energy distribution from the accelerator value 1.5×10^{-4} to 1.7×10^{-4}. The target thickness sufficed to reach the equilibrium charge state distribution. The distribution measured in this experiment is Gaussian ($Q=47,\sigma=1.5$) and in excellent agreement with theoretical calculations [15] (Fig. 2).

Figure 3 shows the energy distribution in the ionization chamber as a function of the horizontal position in the second drift chamber, for ^{125}Te ions scattered at $\theta_{\mathrm{Cex}}=2.6°$. There are four kinds of events. The position in the drift chamber of the events labeled (1) depends on the magnetic field. The distribution of these events reflects the energy straggling distribution of the Te ions leaving the target. For a given charge state, the events labeled (2) are at the same position in the drift chamber, but have different energies in the ionization chamber. This energy distribution reflects the energy degradation in the detector windows after passing through the magnetic field. The events labeled (3) are mainly due to pileup of events inside the drift chamber. The events labeled (4) have the same energy independent of the charge state, but have different X positions corresponding to different trajectories caused by a change of the ionic charge state in the magnetic field. These events are of main interest in this experiment and are included in the contour gate shown in the figure, called E_{ic}, set on the elastic events.

Figure 4 gives a scatter plot of the ion positions in the two drift chambers ($X1$, $X2$). A contour gate is also set on the events distributed along a straight line corresponding to the angle of emergence θ from the last quadrupole.

The effect of the contour gates on the background is very drastic, as shown in Fig. 5. The figure compares the ungated horizontal distribution (dotted lines) with that gated by the contours E_{ic} and θ defined in Figs. 3 and 4. Here, the scattering angle was fixed to $\theta_{\mathrm{Cex}}\leqslant0.2°$ for which Coulomb excitation is negligible. The peaks of the different charge states have an asymmetric shape with a low-energy (left side) tail corresponding to the remaining energy straggling in the target. Between these peaks, a few events remain after the gating conditions have been applied, corresponding to the events labeled (4) in Fig. 3. We call $\mathcal{R}$ the ratio of the total counts in an interpeak interval of $n=24$ channels to the event number in the corresponding peak on the right-hand side. We find an approximately constant value of $\mathcal{R}\simeq(0.44\pm0.1)\times10^{-4}$. As the interpeak region is $\sim$160-mm wide and the drift chamber width is 600 mm, only three charge state peaks could be measured at a given magnetic rigidity of the spectrometer.

IV. DATA ANALYSIS AND RESULTS

A. General remarks

Figure 6 gives the θ,E_{ic} gated spectrum of the Te ions in the second drift chamber for a scattering angle $\theta_{\mathrm{Cex}}=2.6°$.

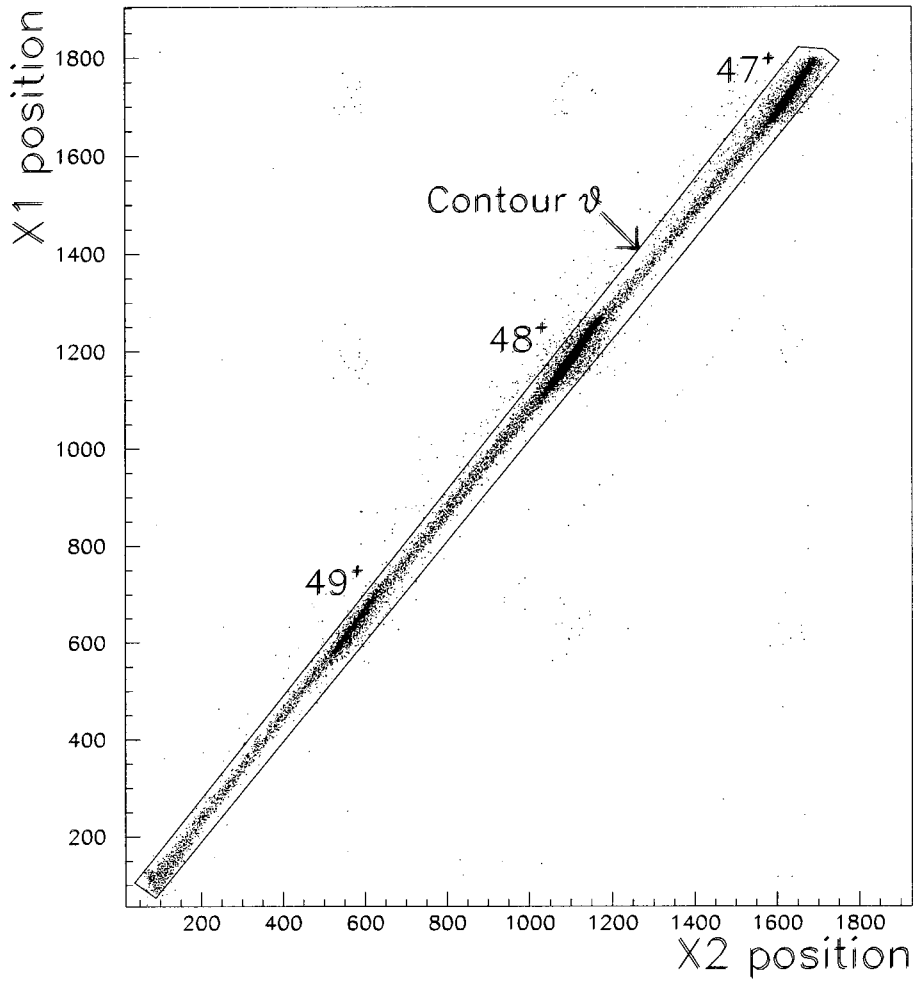

FIG. 4. X position distribution of Te ions in the two drift chambers for charge states 47, 48, and 49 and for a scattering angle $\theta_{\mathrm{Cex}}=2.6°$. The rectangle shows the contour (θ) of $X1$-$X2$ positions used to gate the elastic events.

During the experiment, the magnetic rigidities were tuned in such a way that two consecutive runs had two common charge state peaks in the focal plane. The spectra could thus be added by overlapping the related common peaks.

Inside the magnetic field of SPEG, beyond the distance d from the target, different species of ^{125}Te ions coexist.

(i) ^{125}Te ions in the nuclear ground state, called *parents*, give peaks in the spectra of Fig. 6. This figure presents the horizontal positions in the second drift chamber. The peaks have an asymmetric shape because of the angular dependence of the elastic cross section within the angular opening $\Delta\theta_{\mathrm{Cex}}$. The effect is especially large because of the special tuning and beam focusing of SPEG noted in Sec. III.

(ii) ^{125}Te ions Coulomb excited to the first nuclear state, with a half-life $T_{1/2}^{Q}\simeq t_d$. Following the IC process, an electron is emitted in the continuum, but due to the short lifetime these ions cannot be distinguished from those in their ground state which enter the magnetic field with a charge state $(Q+1)$ [see (i)].

(iii) ^{125}Te ions with excited nuclei and with $T_{1/2}^{Q}>t_d$ which implies $Q\geqslant Q_c$, called *daughters*. At some position inside the magnetic field the nuclear state decays. Part of the decay arises by γ emission, the other by IC and increments the charge state by one unit. The $^{125}\mathrm{Te}^{Q}$ ions become $^{125}\mathrm{Te}^{(Q+1)}$ and their trajectories move towards that of the unexcited incident $Q+1$ ions. Thus they end in the drift chambers at positions between the unperturbed *parent* $^{125}\mathrm{Te}^{Q}$ and $^{125}\mathrm{Te}^{Q+1}$ ion peaks. It is worth noting that the probability of a double charge state change due to the Auger process is very small. In Be-like ions, e.g., with a $1s2s^22p$ configuration, the calculated fluorescence yield is 86% [16]. So for all relevant charge states $Q\geqslant Q_c$, which are those with $T_{1/2}^{Q}>t_d$ (see Sec. V), this process is completely negligible.

The effect of lifetime variation can be seen qualitatively in the spectrum of Fig. 6. The intervals between peaks 44-45, 45-46, and 46-47 reflect only the background: the $\mathcal{R}$ values associated with these charge state intervals are comparable with those obtained at $\theta_{\mathrm{Cex}}\leqslant 0.2°$ (Fig. 5). In contrast, the large values of $\mathcal{R}$ associated with the charge states 47^+, 48^+ are the signature of an enhanced nuclear lifetime. Since the modification of the charge state during the flight produces events located on the high-energy side of the peaks, such events cannot be confused with those produced by energy loss and not eliminated by the gating conditions. The total number and distribution of these events are used to deduce the lifetimes associated with the different charge states.

B. Simulation

A direct analysis of the data is very difficult. To deduce, from the location of an ion in the drift chamber, the location

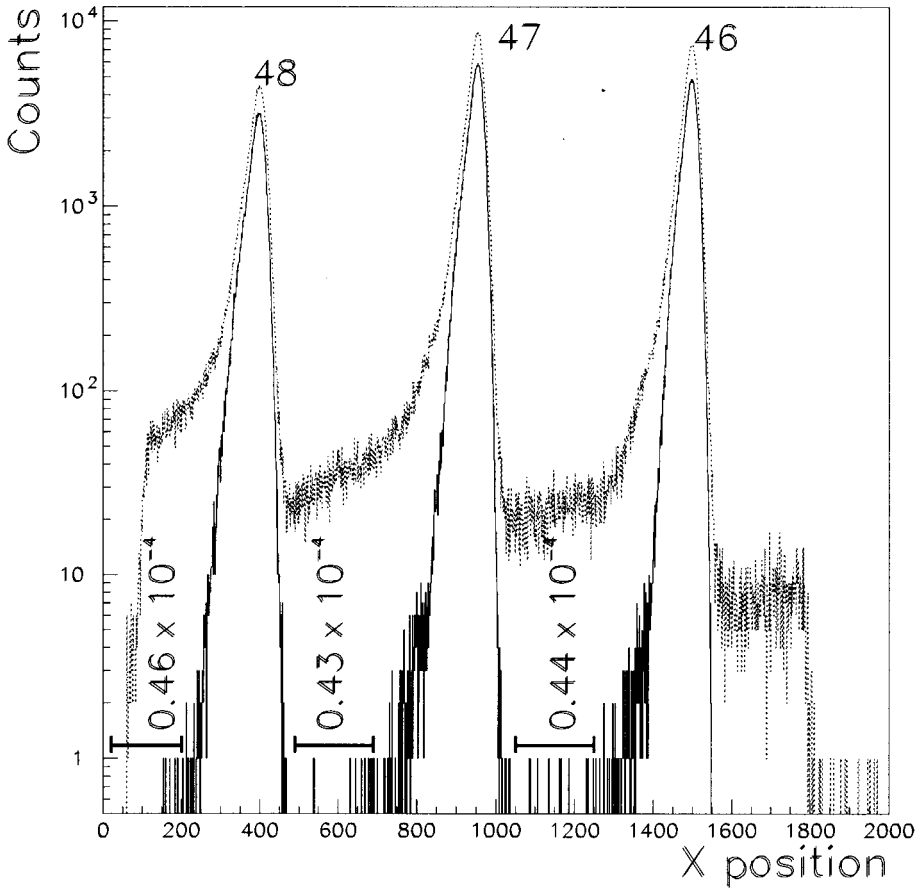

FIG. 5. Experimental horizontal distribution (X) of ^{125}Te ions impinging on a ^{232}Th target and scattered at $\theta_{\mathrm{Cex}} \simeq 0°$. On the ungated spectrum, shown by dotted lines, the spectrum gated by the (θ, E_{ic}) contours is superposed. The ratio $\mathcal{R}$ of the interpeak counts to the counts in the right-hand side peak is indicated. The shape near the top of the peak characterizes the incident beam, while the energy loss in the target produces the tail and the events on the left side of these peaks.

inside the magnetic field where the IC process occurs and the time of the occurrence of the nuclear deexcitation, one needs to reconstruct the actual trajectory through all the magnetic elements. Unfortunately, the relationship between the impact points in the drift chambers and the point of decay is not unique. For example, trajectories at different entrance angles could end up at the same impact point for different decay locations. Therefore, for a quantitative interpretation of the data we developed a simulation program called TURTLE$^+$ [17].

In the simulation we used the following parameters: (i) the beam dispersion parameters ($\Delta X, \Delta Y, \Delta\theta, \Delta\phi, \Delta P/P$) deduced from the analysis of the incident beam; (ii) the scattering angle ($\theta_{\mathrm{Cex}} = 2.6 \pm 0.2°$) given by the slit positions and confirmed by the measurement of the shape of peak tops; (iii) the magnetic rigidity; (iv) the incident angle θ_0 and position X_0 in the spectrometer; (v) a background ratio $\mathcal{R} \simeq 0.5 \times 10^{-4}$ from Fig. 5, assumed to be the actual background because of the very low Coulomb excitation probability at $\theta_{\mathrm{Cex}} \simeq 0.2°$; (vi) a nuclear half-life $T_{1/2}$, arbitrarily fixed for all charge states and then optimized (see below); (vii) for each charge state, the value of the corresponding ICC calculated from the $T_{1/2}$ value and relation (2). (viii) the feeding probability of the first excited nuclear state of 1.3×10^{-3}, evaluated from the known branching ratios and $B(E2)$ values [8,18]. (ix) the experimental charge state distribution. An example of the simulation giving the Te ion distribution in the second drift chamber is shown in dotted lines in Fig. 6(a) for charge states $Q = 44 - 49$. In this example, we used a common half-life value equal to $T^0_{1/2} = 1.486$ ns. There is very good agreement between experiment and the calculated positions, shapes, and intensities of the main peaks. The simulation also reproduces very well the major features of the interpeak data for the 44^+, 45^+, and 46^+ *daughters*. It fails to reproduce those for the 47^+ and 48^+ charge states.

We made simulations with a range of half-lives $T_{1/2}$ between 1.5 and 22 ns. A first set of simulations [dotted curves in Figs. 6(a), 6(b), and 6(c)] was done with a total number of events equal to the experimental one. All the ion trajectories exiting from the target were followed. Due to the very small Coulomb excitation probability this yielded only a small number of charge changed events by IC inside the magnetic field even though this kind of simulation required a large computing time. Nevertheless, this allowed us to evaluate the spectrometer transmission including the effect of the spatial constraints imposed by all the elements in the beam line and the detection system, together with the energy loss and straggling in the target, on the Te distribution.

A second set of simulations followed only the trajectories of *daughter* events, assuming a unit Coulomb excitation probability, thus providing much better statistics in the interpeak regions [boldfaced dashed curves in Figs. 6(b) and 6(c)]. These simulations were normalized to the previous ones which started with *parent* ions.

A quantitative comparison between experiment and the simulation was made over each interpeak interval of $n = 24$ channels, indicated by the horizontal lines in Fig. 6(a), as a

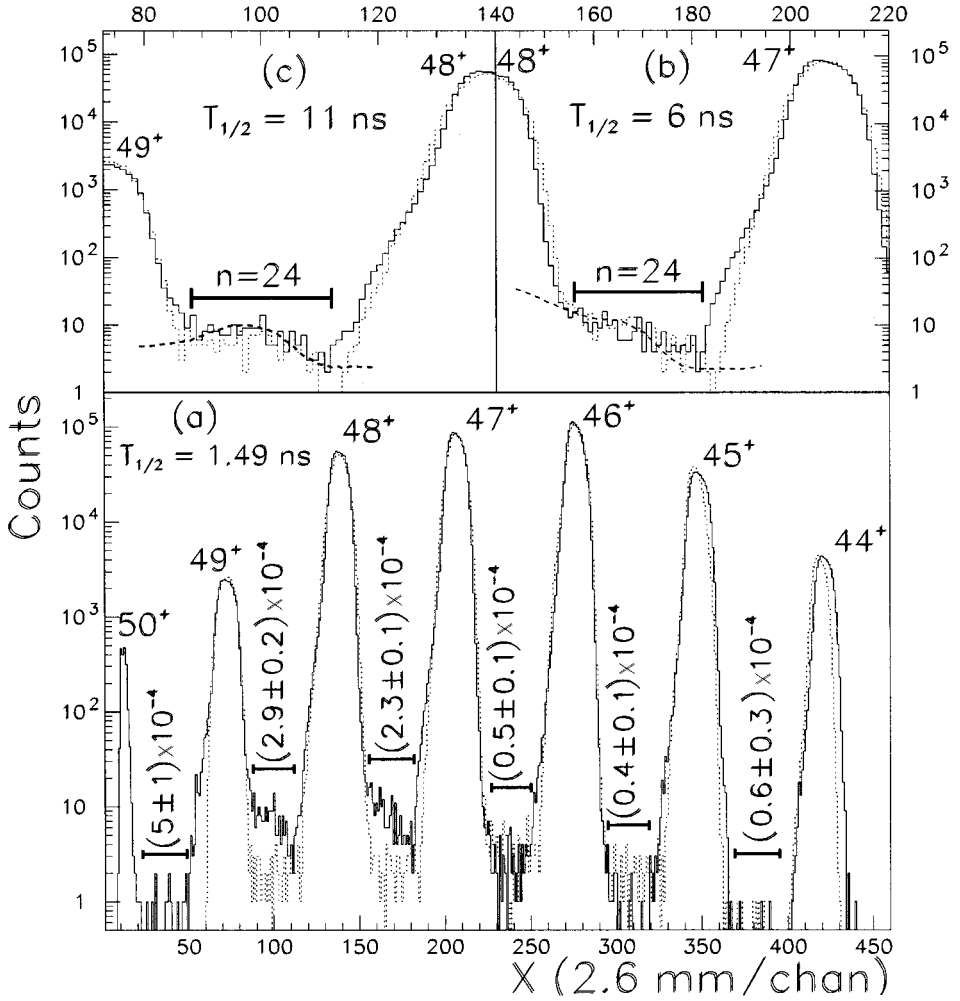

FIG. 6. (a) Experimental horizontal distribution of ^{125}Te ions scattered at $\theta_{Cex}=2.6°$. A simulation in dotted lines is shown only for one Q-independent half-life $T_{1/2}=1.5$ ns. The numbers give the ratios $\mathcal{R}$ of the number of interpeak counts in each selected interval, indicated by a horizontal line, to the counts in the corresponding peak on the right. Separately measured background ratios (see text) for $Q=46$, 47, and 48 are shown in Fig. 5. (b) Expanded interpeak spectra and low- and high-statistics simulations (dotted and dashed, respectively) for $T_{1/2}=6$ ns and for $Q=47$ (see text). (c) Same as (b), but for $T_{1/2}=11$ ns and for $Q=48$.

function of $T_{1/2}$. For each charge state, we calculated the quantity χ^2/n, resulting in the plot of Fig. 7 for $Q=46$, 47, 48. The value of $T_{1/2}$ which minimizes χ^2/n is adopted as the most probable value of the first-excited-state half-life of ^{125}Te nuclei for a given charge state. This minimum value was found to be independent of n within a reasonable range.

The $T_{1/2}$ values and relative one standard deviation uncertainties are listed in Table II. They are compared with theoretical values calculated from the ICC given by the electronic configuration of the atoms (see Sec. V). One sees a spectacular increase of the first excited state half-life beyond $Q=46$, to which we return below.

The ratio $\mathcal{R}$ (Sec. III) can also be used to deduce the half-life. In Fig. 8, we give a scatter plot of the calculated decay lengths Z_d (velocity $\times$ time before IC decay) versus the X positions, for *daughter* ions of charge states $Q=46-49$ and for different half-lives $T_{1/2}=1.49$, 6, 11 ns. The shapes of the decay length distribution for different lifetimes is easily understood: for the short half-lives ($\sim$1.5 ns), Fig. 8(a), a very small fraction of Te ions change their charge state inside the magnetic field of the first dipole of SPEG. When the lifetime increases, a larger fraction of the ions decays in the first dipole and the distribution of events in the drift chamber reflects the exponential decay. For a half-life $T_{1/2}=6$ ns, Fig. 8(b), a significant fraction of ions starts to decay in the drift space between the two magnetic dipoles. Te ions decaying in this region of the spectrometer have the same position in the drift chamber. For a still larger half-life $T_{1/2}=11$ ns, Fig. 8(c), an important fraction of excited Te ions reaches the second dipole. Once more, the X position distribution in the drift chamber follows the exponential decay law. It is seen in Figs. 8(b) and 8(c) that the position of Te^{Q} ions decaying in the second dipole of SPEG can overlap with the position of Te^{Q+1} ions which decay in the first dipole. This gives an experimental limit to the lifetime which can be obtained by this method.

From the preceding discussion, one can understand the shape of the X distribution in the interpeak region, in particular, the approximately bell shaped distribution for $T_{1/2}=11$ ns due to the large fraction of Te ions decaying in the drift region, seen in Fig. 6(c). For a given number of interpeak channels n, the total number of events depends not

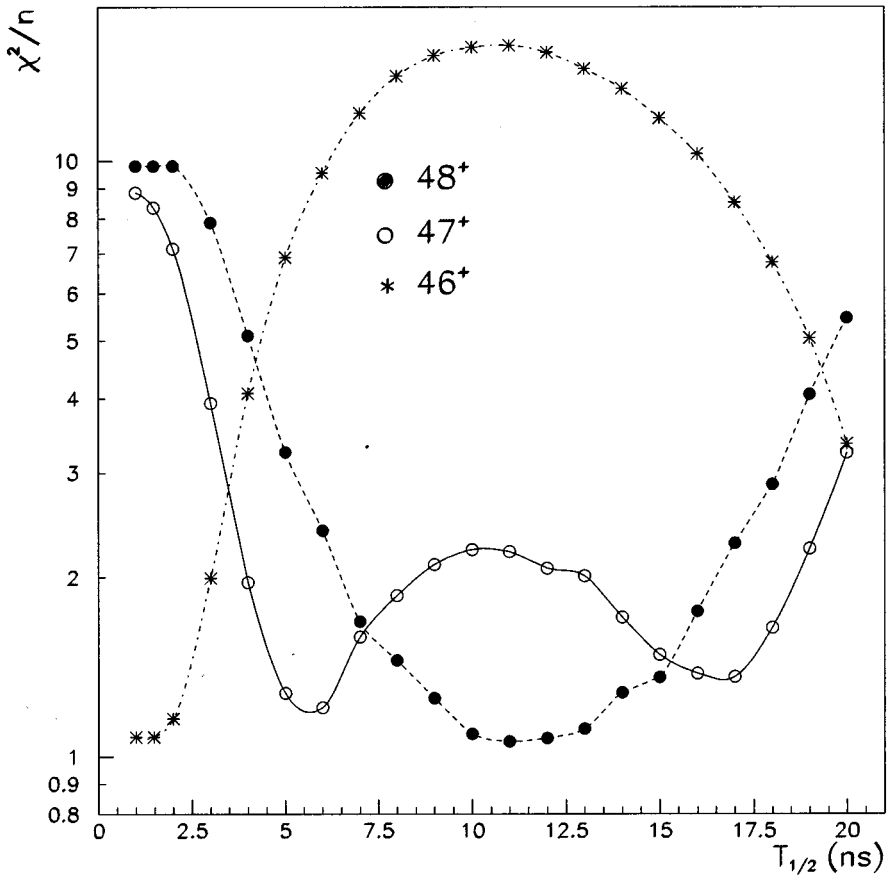

FIG. 7. Distribution of χ^2/n for simulations fitting the experimental distribution in the interpeak regions for $Q=46-48$ as a function of the assumed $T_{1/2}$.

only on the exponential decay law, but also on the absolute value of the ICC (α_T^Q) which is related to the half-life through Eq. (2.2). Large values of $T_{1/2}$ imply small values of α_T^Q and consequently few decaying ions. The ratio $\mathcal{R}$, as previously defined, is thus a function of the two variables $T_{1/2}$ and Q.

Taking into account the background contribution in the interpeak interval, the values of $\mathcal{R}$ for different $T_{1/2}$ and Q values are plotted in Fig. 9. One sees that for a given experimental value of $\mathcal{R}$, two solutions for $T_{1/2}$ are possible (very short and long half-lives both produce few interpeak counts). One solution typically can be rejected on the basis of physical argumentation. Also the shapes of the X distributions are very different for the possible solutions. For $Q=48$ the relative uncertainty is rather large. From the figure one can deduce the values of $T_{1/2}^Q$ listed in Table II, which are in good agreement with those found by the χ^2/n method.

TABLE II. Half-lives of the first excited nuclear state of ^{125}Te for various ionic charge states.

Charge state	$T_{1/2}$ (ns) Exp.[b]	Exp.[c]	Calc.[d]	Calc[e]
0			1.486(9)[a]	
44		~ 1.5	1.60	1.65
45		$\leqslant 1.5$	8.0	2.6
46	$\leqslant 2$	1.8 ± 0.4	8.3	6.7
47	6 ± 1	5.9 ± 0.5	8.5	7.9
48	11 ± 2	11.0 ± 2.5	10.3	10.1

[a]Experimental value, used in Eqs. (2) and (3). The uncertainty in the last digit is shown in parentheses.
[b]Obtained by the χ^2/n method (see text).
[c]Obtained by the $\mathcal{R}$ ratio method (see text).
[d]Without inclusion of BIC.
[e]With inclusion of BIC [22].

V. INTERPRETATION OF THE RESULTS

The IC process is sensitive mainly to the electronic wave function close to the nucleus. This property can be used to determine the ICC in an ionic system of charge state Q (α^Q) from the ICC in neutral atoms (α^0) [20,21]. For a nonrelativistic system, one finds [19]

$$\alpha^Q = \alpha^0 \lim_{r\to 0} \frac{\rho^Q(r)}{\rho^0(r)}, \tag{5.1}$$

where $\rho(r)$ is the electronic density in the nuclear region.

Any variation in the configuration of the outer electronic shells induces a modification of the screening and thus a modification of the inner electron wave functions. Nevertheless, the resulting modification of the electronic density near the nucleus is small for the electrons in the 1s shell. This leads to a small variation of the K-shell ICC with Q, as found for ^{57}Fe ions with charge states $Q=19-23$ [6]. This is also the reason of the small expected change in the lifetime of Te ions in the charge state $Q=44$ compared to $Q=0$ (Table II).

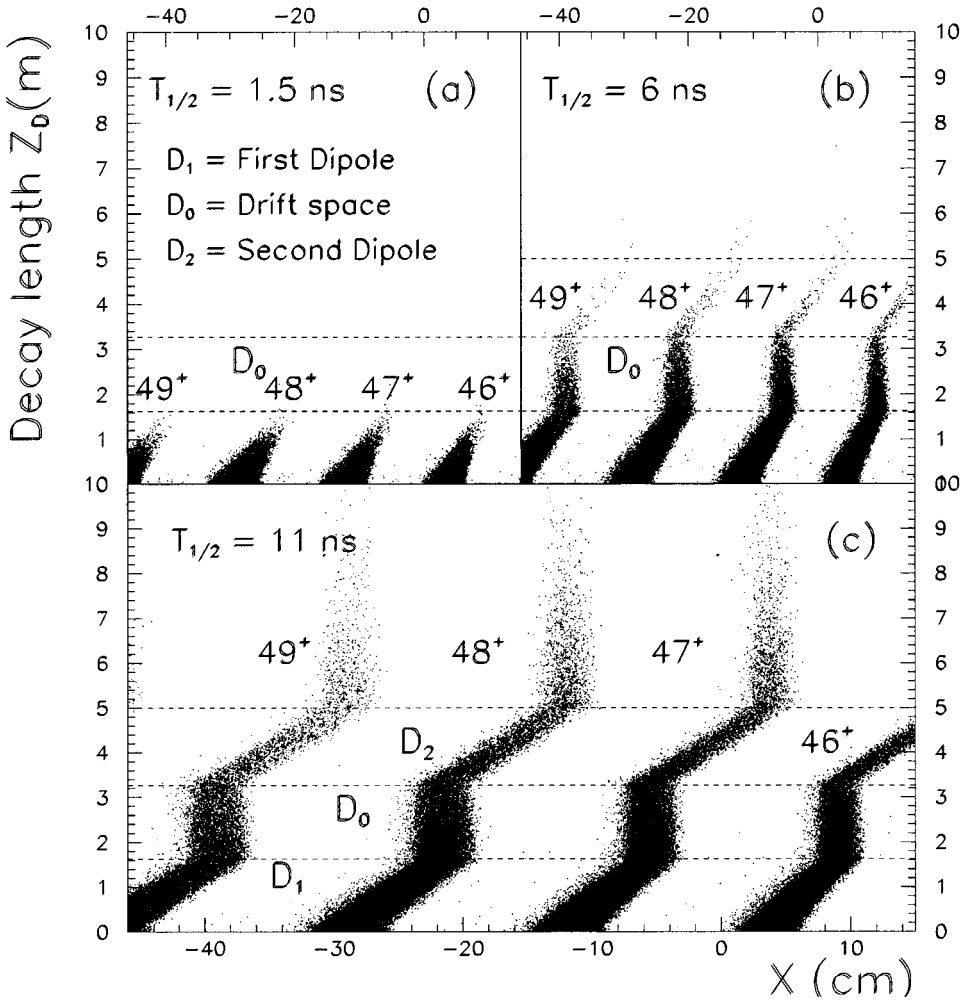

FIG. 8. Simulation of the decay length distributions as a function of the ion positions in the second drift chamber, for the charge states $Q=46$-49 and for half-lives $T_{1/2}=1.5$, 6, and 11 ns. The simulations are given for the same total number of decaying ions for the different charge states.

Assuming that the IC process of the K shell is totally inhibited if the transition energy becomes smaller than the binding energy of the K-shell electrons, the expected lifetimes can be obtained from Eq. (2.2), using calculated values of α_T^Q [19,22]. In Tables II and III, we report these calculated values of $T_{1/2}^Q$ and α_T^Q, respectively, together with the experimental values. The agreement is good for the charge states $Q=44$, 47, and 48, but large discrepancies are seen for $Q=45$ and 46. For the latter, the experimental lifetimes are very close to the neutral-atom lifetime. To explain this finding, in Ref. [7] we suggested that IC could in principle take place between two atomic bound states in excited Te ions, a process we called *bound internal conversion* (BIC).

Recent calculations [23] show that ICC values indeed do not change significantly when the nuclear transition energy crosses the $(1s)$ electron continuum threshold energy value. For a transition to a bound state labeled by the relativistic quantum numbers n,κ, IC becomes a resonant process with an ICC value of

$$\alpha_{n\kappa}^b = r_{n\kappa}\frac{1}{2\pi}\frac{\Gamma}{(\omega_\gamma-\omega_{n\kappa})^2+(\Gamma/2)^2}, \qquad (5.2)$$

where Γ is the total width of the electron hole state produced by the IC, ω_γ is the nuclear transition energy, $\omega_{n\kappa}$ is the excitation energy of the hole state, and $r_{n\kappa}$ is analog to the usual ICC, but normalized on the energy scale. Just below the continuum boundary the density of atomic states is large and the probability to find available states in an energy range of $\omega_\gamma \pm \Gamma/2$ is close to unity. For K-shell conversion in ions having p electrons, the radiative width of the excited state is dominated by emission of $2p \rightarrow 1s$ x rays (in ^{125}Te, one finds for the ratio Auger rate/radiative rate $\sim 10^{-2}$ [16]). For Te ions with one or two p electrons, such a decay gives $\Gamma \simeq 5$ eV. Using Eq. (5.2), modified ICC values can be obtained, as follows.

$Q=45,46$. As there is no metastable electronic configuration remaining after 1.5 ns [12], the total ICC, including the probability of bound IC $\alpha^{b,Q}$ are respectively equal to

$$\alpha_T^{45} = \alpha_K^{b,45} + \alpha_{L1}^{45} + \alpha_{L2}^{45} + \frac{1}{4}\alpha_{L3}^{45} = 7.5,$$

$$\alpha_T^{46} = \alpha_K^{b,46} + \alpha_{L1}^{46} + \alpha_{L2}^{46} = 2.3.$$

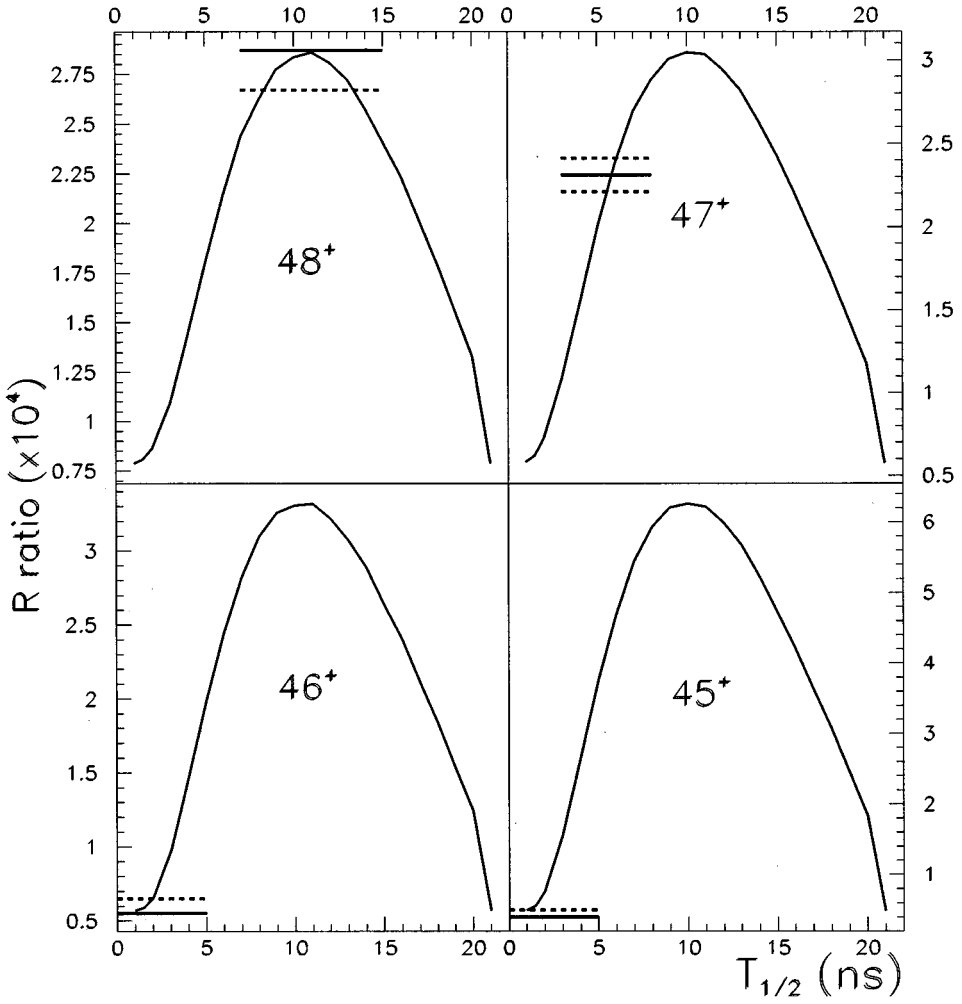

FIG. 9. Distribution of the calculated ratio $\mathcal{R}$ versus the half-life $T_{1/2}$. The experimental values of $\mathcal{R}$ are drawn in boldface lines and their uncertainties in dashed lines.

$Q=47$. B-like ^{125}Te ions also have no metastable electronic configuration with a lifetime larger than 1.5 ns. The ICC value of the ground state configuration is

$$\alpha_T^{47}=\alpha^{b,47}+\alpha_{L1}^{47}+1/2\alpha_{L2}^{47}=1.8.$$

$Q=48$. For Be-like Te, there is the well-known $^3P_0$ metastable configuration with a lifetime of about 10^{-3} s [24]. Assuming a statistical population of the ten different Be-like configurations at the target exit, inside the spectrometer this beam consists of ions 59% in the $(2s^2)^1S_0$ ground state and 41% in the $(2s2p)^3P_0$ excited state [25]. We deduce a mean ICC for the two configurations,

$$\alpha_T^{48}=\alpha_L^{48}\simeq 1.0.$$

TABLE III. Internal conversion coefficients of the first excited nuclear state of ^{125}Te for various ionic charge states.

Charge state	α_K^Q Calc.[d]	α_K^Q Calc.[e]	α_K^Q Exp.[b]	α_T^Q Exp.[c]	α_T^Q Calc.[d]	α_T^Q Calc.[e]
0	11.985(7)[a]		13.912(1)[a]		13.912(1)[a]	
44				~13	13.2	
45	0	5.9		⩾13	1.8	7.5
46	0	0.6	⩾13	11±2	1.7	2.3
47	0	0.20	2.7±0.5	2.7±0.2	1.6	1.8
48	0	0	1.0±0.2	1.0±0.2	1.1	1.0

[a]Experimental values. The uncertainty in the last digit is shown in parentheses.
[b]Calculated from Eq. (2) and $T_{1/2}$ using the χ^2/n method (see text).
[c]Calculated from Eq. (2) and $T_{1/2}$ using the $\mathcal{R}$ ratio method (see text).
[d]Without inclusion of BIC.
[e]With inclusion of BIC [22].

These values of the ICC were used in Eq. (2.2) to calculate the expected half-lives listed in Table II. One notes the great improvement for $Q=45$ whose calculated $T_{1/2}$ value is now close to the experimental one. For $Q=46$, a discrepancy remains, much smaller than without BIC. However, in this K-shell binding energy range the ICC is very sensitive to any small variation of either ω_γ or binding energies [23]. For example, a change of 23 eV of the electronic transition energy ω_γ, changes $\alpha_K^{b,46}$ from 0.262 to 161. An energy shift of 66 eV would give a resonance on the $7s$ level of Te^{47+} with a value of $\alpha_K^{b,47}=760$ instead of the quoted value $\alpha_K^{b,47}=0.2$.

VI. CONCLUSION

We have presented in detail an experiment leading to a very large ionic-charge state dependence of the first excited state lifetime in ^{125}Te nuclei which decay mainly by internal conversion. We found a large increase of this halflife from the charge state $Q=47$ onwards, whereas it was expected theoretically from $Q=45$ onwards, for which the calculated K-shell binding energy exceeds the nuclear transition energy [7]. As the energies and the experimental charge states are well determined, we assert that only the assumption of a K-shell internal conversion process into atomic bound states (*bound internal conversion*) can explain our findings. The calculations made within this assumption [23] give half-life values in better agreement with the experimental values. These effects are not restricted to ^{125}Te ions but should apply to any ion undergoing internal conversion decay, as soon as its charge state is high enough so that the K-shell binding energy exceeds the nuclear transition energy.

ACKNOWLEDGMENTS

It is a pleasure to acknowledge the support of the CENBG and GANIL technical staffs and in particular the technical assistance around SPEG. One of us (W.E.M.) acknowledges partial support by National Science Foundation Grant No. PHY-9019293 (Stanford University).

[1] G. T. Emery, Annu. Rev. Nucl. Part. Sci. **22**, 165 (1972).
[2] K. Takahashi and K. Yokoi, At. Data Nucl. Data Tables **36**, 375 (1987); Phys. Rev. C **36**, 1522 (1987).
[3] H. Ulrickson, R. Hensler, D. Gordon, N. Benczer-Koller, and H. DeWaard, Phys. Rev. C **9**, 326 (1979).
[4] M. Jung, F. Bosch, K. Beckert, H. Eickhoff, H. Folger, B. Franzke, A. Gruber, P. Kienle, O. Klepper, W. Koenig, C. Kuzhuharov, R. Mann, R. Moshammer, F. Nolden, U. Scharf, G. Soff, P. Spädtke, M. Steck, Th. Stöhlker, K. Sümmerer, Phys. Rev. Lett. **69**, 2164 (1992).
[5] R. Daudel, M. Jean, and N. Lecoin, J. Phys. Radium **8**, 238 (1947).
[6] W. R. Phillips, I. Ahmed, D. W. Banes, B. G. Glagola, W. Henning, W. Kutschera, K. E. Rehm, J. P. Schiffer, and T. F. Wang, Phys. Rev. Lett. **62**, 1025 (1989); Phys. Rev. A **47**, 3682 (1993).
[7] F. Attallah, M. Aiche, J. F. Chemin, J. N. Scheurer, W. E. Meyerhof, J. P. Grandin, P. Aguer, G. Bogaert, C. Grunberg, J. Kiener, A. Lefebvre, and J. P. Thibaud, Phys. Rev. Lett. **75**, 1715 (1995).
[8] J. Barrette, H. Barrette, R. Harroutunian, G. Lammoureux, S. Monaro, and S. Markiza, Phys. Rev. C **11**, 282 (1975).
[9] W. M. Roney, D. W. Gebbie, and R. R. Borchers, Nucl. Phys. **A236**, 165 (1974).
[10] J. P. Miller, F. Boehm, and H. E. Henrikson, Nucl. Instrum. Methods **136**, 403 (1976).
[11] W. B. Walters and R. A. Meyer, Phys. Rev. C **145**, 1925 (1976).
[12] F. Attallah, ''Variation des Périodes Radioactives en Fonction de L'état de Charge Atomique: Cas du ^{125}Te'' (''Nuclear Lifetime Variation as a Function of the Atomic Charge State: Case of ^{125}Te''), Ph.D thesis, University of Bordeaux I, Report No. CENBG 9430 (1994) (unpublished).
[13] P. Indelicato (private communication).
[14] L. Bianchi, B. Fernandez, J. Gastebois, A. Gillibert, W. Mittig, and J. Barrette, Nucl. Instrum. Methods Phys. Res. A **276**, 509 (1989).
[15] J. P. Rozet, ETACHA (version 9-94), Program for Heavy-ion Charge Distributions (private communication).
[16] M. H. Chen and B. Crasemann, Nucl. Phys. **A35**, 4579 (1987).
[17] F. Attallah, J. F. Chemin, and J. N. Scheurer, TURTLE+: Trace Unlimited Rays Through Lumped Elements, Internal Report No. CENBG 941, CENBG, France, 1994, CERN Library, 1994 (unpublished).
[18] H. Sergolle, G. Albony, J. M. Lagrange, M. Poutrat, N. Paffé, and J. Vanhorenbeek, Nucl. Phys. **A145**, 351 (1970).
[19] I. M. Band, L. A. Sliv, and M. B. Trzhaskovskaya, Nucl. Phys. **A156**, 170 (1970).
[20] L. A. Sliv, JETP **21**, 790 (1951); I. A. Sliv and I. M. Band, in *Alpha, Beta and Gamma-ray Spectroscopy*, edited by K. Siegbahn (North-Holland, Amsterdam, 1979), p. 1639.
[21] F. Rösel, H. M. Fries, K. Alder, and H. C. Pauli, At. Data Nucl. Data Tables **21**, 92 (1978).
[22] Hartree-Fock calculation. F. Karpeshin (private communication).
[23] F. F. Karpeshin, M. R. Harston, F. Attallah, J. F. Chemin, J. N. Scheurer, I. M. Band, and M. B. Trzhaskovskaya, Phys. Rev. C **53**, 1640 (1996).
[24] J. P. Marques, F. Parente, and P. Indelicato, Phys. Rev. A **47**, 929 (1993).
[25] M. Harston, GRASP program calculations (private communication).
[26] G. Zschornack, G. Musiol, and W. Wagner, ''Dirac-Fock-Slater X-ray Energy Shifts and Electron Binding Energy Changes for all Ion Ground States in Elements up to Uranium,'' Report No. ZfK-574, Institute for Nuclear Physics, Rossendorf/Dresden, Germany, 1986 (unpublished).
[27] W. R. Phillips, GRASP program results (private communication).
[28] J. A. Bearden and A. F. Burr, Rev. Mod. Phys. **39**, 125 (1967).